VIII International Conference on Fracture Mechanics of Concrete and Concrete Structures
FraMCoS-8
J.G.M. Van Mier, G. Ruiz, C. Andrade, R.C. Yu and X.X. Zhang (Eds)

EVALUATION OF CRACK PROPAGATION IN ASR DAMAGED CONCRETE BASED ON IMAGE ANALYSIS

TOMOHIRO MIKI*, KOICHIRO MATSUTANI† AND YUDAI MIYAGAWA†

* Kobe University, Department of Civil Engineering
1-1 Rokkodai, Nada, Kobe, JAPAN
e-mail: mikitomo@port.kobe-u.ac.jp, web page: http://www2.kobe-u.ac.jp/~mikitomo/
†Kobe University, Department of Civil Engineering

Key words: Alkali Silica Reaction, Tension Softening Curve, Fracture Energy, Strain Distribution

Abstract: This study presents an investigation to evaluate the crack propagation in the cracked concrete that is damaged due to alkali-silica reaction (ASR). We obtained the fracture energy and tension-softening curves of the ASR damaged concrete. Three-point bending tests for single notched concrete beams were carried out to determine the fracture properties. To detect the crack propagation behavior, an image analysis by using a digital image correlation method was carried out. In this method of image analysis, a region-based matching technique is used to calculate the displacement of any portion of the concrete surface. As for the macroscopic damage in the concrete the ASR induced cracks that can be observed on the surface of concrete were evaluated and classified into their widths, lengths and directions. The experiments show that these ASR-induced cracks affect on the crack propagation in the specimen under the bending.

1 INTRODUCTION

Alkali-silica reaction (ASR) in the concrete is a phenomenon that alkali ingredients such as reactive silica in the aggregate react with the sodium hydroxide in the cement. This reaction sometimes results in gel that causes the volume expansion of concrete and then the crack may occur in the concrete. The ASR-damaged concrete with cracks has the different mechanical properties from the sound concrete. The reduction of the elastic modulus of concrete is remarkably observed according to the expansion due to the ASR. On the other hand, the compressive strength of ASR-damaged concrete slightly decreases even if the expansion proceeds. The previous research [1] indicates however that the compressive strength of ASR-damaged concrete decreases to about 60% with the expansion of 5000μ. There is room for argument for the influence of the ASR induced crack on the mechanical properties of the concrete.

Furthermore, it is a problem when the phenomenon of the ASR-damaged concrete is evaluated that position and width of the ASR induced cracks have an irregularity which cannot be observed in the sound concrete. Since the ASR induced cracks influence cracks to occur under the external loading, the fundamental data on the mechanical properties of the ASR-damaged concrete are necessary.

In this study, the tension-softening behavior of ASR damaged concrete is experimentally evaluated. Three-point bending test for single notched concrete beams was carried out to determine the fracture properties. These fracture properties are determined from the propagation of mode I crack in the bending test on the concrete beams. This is based on an assumption that the microscopic damage in the concrete is located in the interface of the matrix to both fine and coarse aggregates and

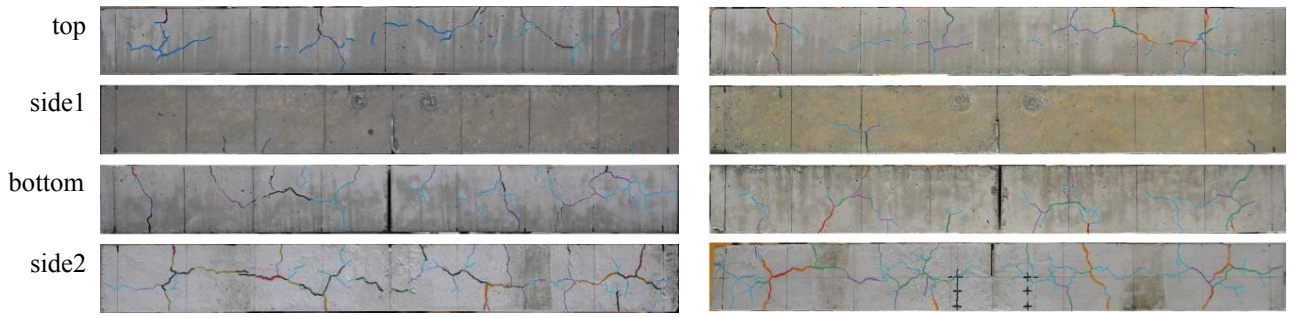

(a) ASR1 (b) ASR2

Figure 1: Distribution of ASR cracks on the specimens

uniformly distributed through the beam.

The previous study presented by the authors [2-4] has showed that he strain distribution obtained by the image analysis can be measured the cracking behavior on the concrete surface under the external load. To detect these crack propagation behavior, an image analysis was carried out during the loading test in order to measure the strain distribution on the concrete beam. As for the macro damage in the concrete the ASR induced cracks that can be observed on the concrete surface are evaluated and classified into their widths, lengths and directions.

2 EXPERIMENT OUTLINES

2.1 Specimens

The concrete specimens is a beam in which the section is 100 mm of width, 50 mm of a ligament hight and 840 mm of the total length. The specimen has a single notch at the midspan whose depth is set as 50 mm. Three specimens were prepared in this experiment. For these specimens, three-point bending test was carried out. Each specimen was made by the same concrete mix. The situation of ASR induced cracks, however, was different because of variability of the material and exposure condisions as shown in **Figure 1**. The mix proportion of this concrete is showed in **Table 1**. Ordinary portland cement for cement and AE water reducing agent for admixture were used. The maximum size of cause aggregate is 20 mm. Both fine and coarse aggregates were mixed where the ratio of reactive and nonresponsive aggregates in the volume of 1:1. The exposure period of the specimen was three years. The upper exposure side is “side2” that is shown in **Figure 1**. In this study, the compressive strength measured with using cylinder specimens having a diameter of 100 mm and a height of 200mm, which is same specified concrete mix as beam specimens, was 31.6 N/mm^2 and the tensile strength was 2.90 N/mm^2.

2.2 Three-point bending test

The loading setup in the experiment is

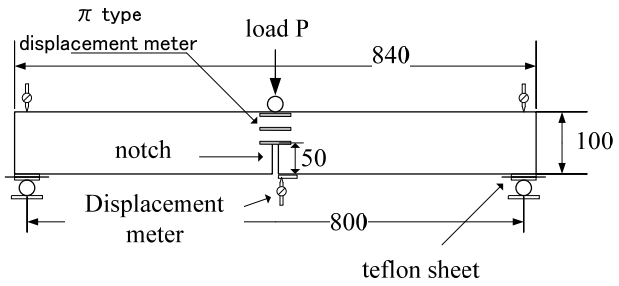

Figure 2: Outlines of the loading test

Table 1: Mix proportion of the concrete

G_{max} (mm)	slump (cm)	W/C %	Air %	s/a %	kg/m^3							
					W	C	S_n	S_r	G_n	G_r	NaCl	AE water redu. agent
20	18	63	5	48	181	287	422	432	466	475	12.4	575 ml

S_n: no-reactive fine aggregate, S_r: reactive fine aggregate,
G_n: no-reactive aggregate, G_r: reactive aggregate

illustrated in **Figure 2**. During the loading test, the load, displacements at both supports and midspan, crack opening displacements, and digital images for an image analysis were measured. For the purpose of the friction reduction at each support, a set of Teflon sheets lubricated with grease was used. The crack opening displacement in the ligament was measured using π-shape displacement transducers. In order to consider the elastic energy released in a bulk part in the specimen when the tension-softening curve was calcurated, reversed cyclic loading was performed.

2.3 Image analysis

In this study, to detect these crack propagation behaviour, an image analysis by using a digital image correlation method [5] was carried out during the loading test in order to measure the strain distribution on the concrete beam. In this method of image analysis, region-based matching technique is used to calculate the displacement of any portion of the concrete surface. The correlated region of dozens of pixel (50 to 100 pixels were set) in the digital pictures which is obtained before/after the deformation under loading is search based on the distribution of the luminance values. In addition, the accuracy of location of the searched region is assumed based on the sub-pixel error cancellation [6].

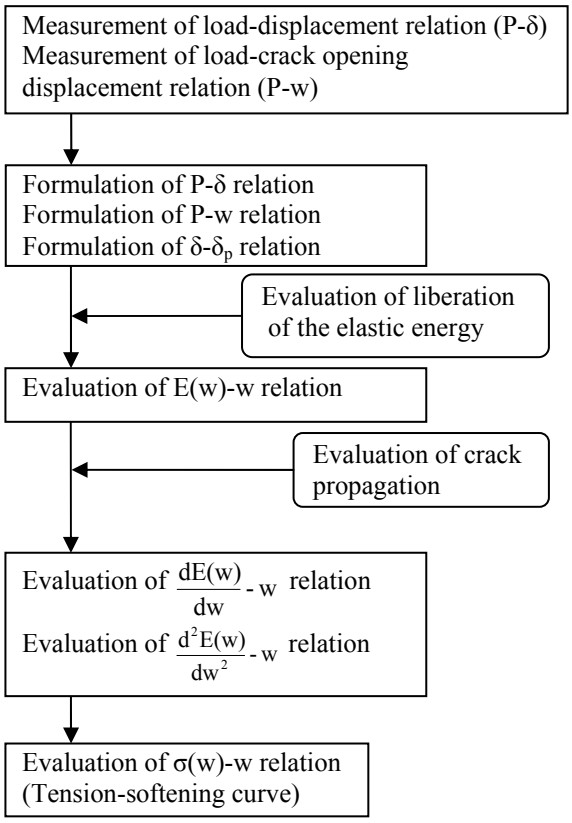

Figure 3: Flow of the extended J-integration method

To take a digital image using a single-lens reflex camera, three-dimensional information is reflected to a two-dimensional image through a camera lens of the camera. In addition, a distortion occurs in the digital image because of the curvature of the lens. Therefore it is necessary to remove a distortion due to the lens curvature, and then the camera calibration to reduce the lens distortion is required in performing the image analysis [4].

From distance between a coordinate in the digital image before the loading and that in an arbitrary loading, the displacement of a target point is calculated. Using the isoparamtric finite element that has nodal points of the target point, the strain distribution in the finite element is interpolated according to the deformation under the loading. In this study, maximum principal strain at each load level is observed to evaluate crack propagation behavior.

2.4 Determination of the tension-softening curve

In order to determine the tension softening curve, the poly-linear approximation method proposed by Kitsutaka et al. [7], and the extended J-integration method proposed by Niwa et al. [8] were used. The extended J-integral method [8] is one of the way to obtain the tension-softening curve of concrete based on the energy balance. This method has improved problems in the modified J-integral method of Uchida et al. [9]. Now following two assumptions were pointed out [8] as problems of the modified J-integral method.

(a) All the energy given as an external work is cosumed at a fictitious crack department
(b) Fictitious crack width progresses under the loading immediately throughout a ligament

Regarding to the assumption (a), in the modified J-integral method, the energy to be

given as the external work is assumed to consume at the fictitious crack. In order to evaluate the energy consumed in the fictitious crack appropriately, the elastic energy released in the bulk part of the beam during unloading is considerd. The factual energy consumed at a fictitious crack department, E(w) can be calcurated as following **Equation (1)**. In this formula, the second term explains the release of the elastic energy.

$$E(w) = \int_0^{\sigma} P(\delta)d\delta - \frac{1}{2}P(\delta)\left(\delta - \delta_p\right) \qquad (1)$$

where, w: the crack opening displacement (mm), E(w): the energy consumed in crack opening displacement w (N·mm), δ: the displacement (mm), P(δ): the load at the displacement, δ(N), δ_p: the plastic displacement under complete unloading (mm)

As for the point (b), when the propagation of the fictious crack is considered since the fictious crack gradually progresses with an increase in the load, the tension-softenning stress σ(w) is evaluated in **Equation (2)**.

$$\sigma(w) = \frac{1}{ab}\left\{2\frac{dE(w)}{dw} + w\frac{d^2E(w)}{dw^2}\right\} \qquad (2)$$

where, σ(w): the tension-softening stress at a crack opening displacement, w (N/mm^2), a: the fictitious crack length (mm), b: the specimen width (mm)

The culculation flow of the extended J-integration method [8] is shown in **Figure 3**.

3 RESULTS AND DISCUSSION

3.1 Tension-softening curve

The tension-softening curves obtained from

Table 2: $\delta - \delta_p$ expression of relations

case	δ_p
refference	$1.42\delta_{max}*(\delta/\delta_{max})^{1.7}$
No.1	$\delta_{max}*(\delta/\delta_{max})^{1.4}$
No.2	$\delta_{max}*(\delta/\delta_{max})^{1.3}$
No.3	$\delta_{max}*(\delta/\delta_{max})^{1.2}$

δ_{max}: maximum displacement (mm)

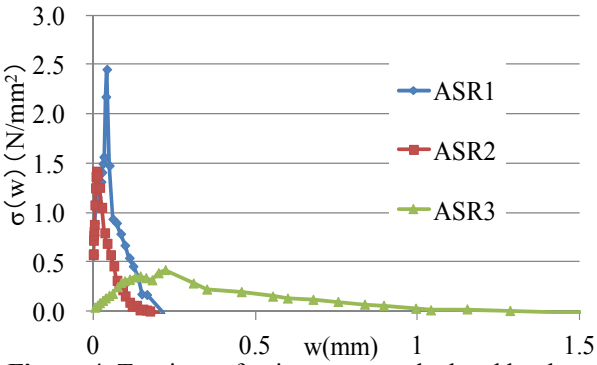

Figure 4: Tension softening curves calculated by the extended J-integration method

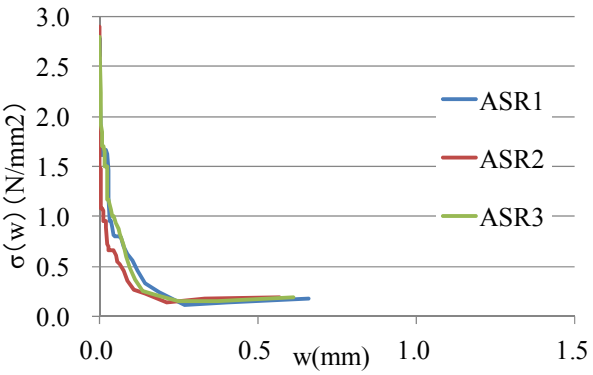

Figure 5: Tension softening curves calculated by the poly-linear approximation method

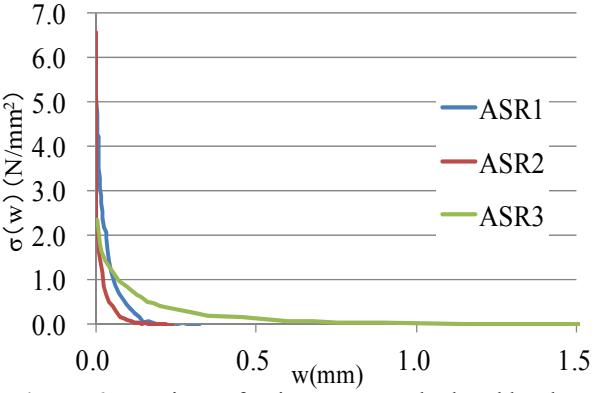

Figure 6: Tension softening curves calculated by the extended J-integration method in which the elastic energy absorption is ignored

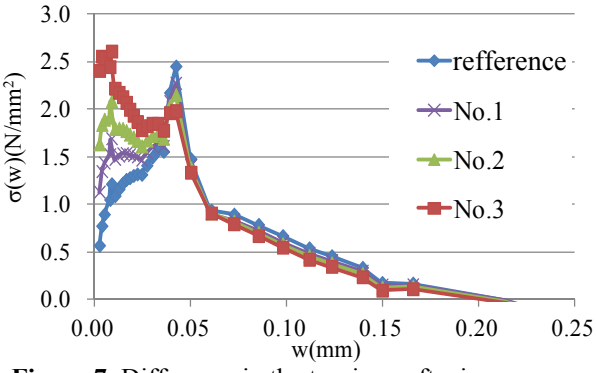

Figure 7: Difference in the tension-softening curves calculated in which different $\delta - \delta_p$ relations are used for specimen ASR1

the three-point bending tests are summarized in this section. **Figures 4 and 5** show the results using the extended J-integration method and the poly-linear approximation method that are mentioned above, respectively. **Figure 4** indicates that the peak tensile stress of the all specimens is larger than the initial stress that corresponds to the tensile strength. On the other hand, for the tension-softening curves obtained from the poly-linear approximation method, the initial stress is of the peak and the tension-softening stress decreases as the increase in the crack width as shown in **Figure 5**.

In this study the fracture properties are assumed to be determined from the propagation of mode I crack in the bending test on the notched concrete beams. This is based on an assumption that the microscopic ASR damage in the concrete is uniformly distributed through the beam. Here, for the tension-softening curve calculated by the extended J-integration method, the elastic energy release during unloading is ignored and the result is shown in **Figure 6**. It is observed that the tension-softening curves shown in **Figure 6** are similar to that obtained by the poly-linear approximation method as shown in **Figure 5**. This is because that in case of the ASR-damaged concrete the elastic energy released in a bulk portion except for the ligament is apparently overestimated, while the energy consumed in the fictitious crack may be underestimated. Therefore, it is necessary to reconsider the elastic energy release of the bulk portion except for the ligament.

Here, to examine the influence of the elastic energy release in the bulk on the tension-softening curves in the case of calculation using the extended J-integration method, a parametric analysis is performed. As an example of the results the tension softening curves of specimen ASR1 are shown. **Table 2** is summarized a series of δ-δ_p expressions that we set in this demonstration. The reference is the expression to fit approximately with the experimental result of load-displacement relations while the cases from No. 1 to No. 3 varies in the plastic displacement, δ_p under the complete unloading. **Figure 7** is the results of the parametric analysis for the tension-softening curve calculated by the extended J-integration method using several δ-δ_p relations. From the comparison of the reference to the each case, as δ_p becomes smaller that is from No.1 to No.3, it turns out that the initial tensile stress becomes larger. In addition, the tension softening curves are approximately similar each other when the fictitious crack width is larger than around 0.05 mm. Therefore, to evaluate the initial tensile stress in the tension-softening curve and the crack propagation behavior just after softening starts, it is important to appropriately evaluate the energy absorption at the crack propagating through the ligament portion.

3.2 Fracture energy

The fracture energy G_F measured in each specimen is summurize in **Table 3**. Here, the G_F is determined from **Equation (3)**.

$$G_F = (W_0 + mg \cdot \delta_{max})/A_{lig} \qquad (3)$$

where, W_0: the area under the load-displacement curve (N·mm), mg: the specimen weight (N), δ_{max} : the maximum displacement (mm), A_{lig}: the cross-sectional area of the ligament (mm^2)

It is found from the results of the G_F that the specimen ASR3 shows largest value of G_F in all specimens. This is because of that the maximum crack width, w_{cr} that was measured at the state in which the bending stress becomes zero in the loading test was the largest as shown in **Figures 4 and 6**.

3.3 Influence of the length and area of the ASR induced cracks

As for the macroscopic damage in the concrete the ASR-induced cracks that can be observed on the surface of concrete are

Table 3: Fracture energy, G_F

specimen	G_F (N/mm)
ASR1	0.168
ASR2	0.090
ASR3	0.202

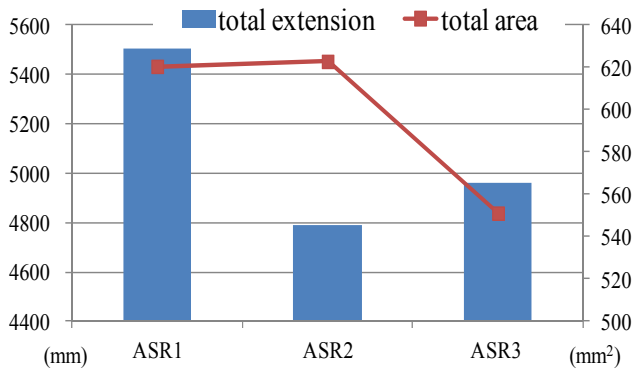

Figure 8: ASR crack situation

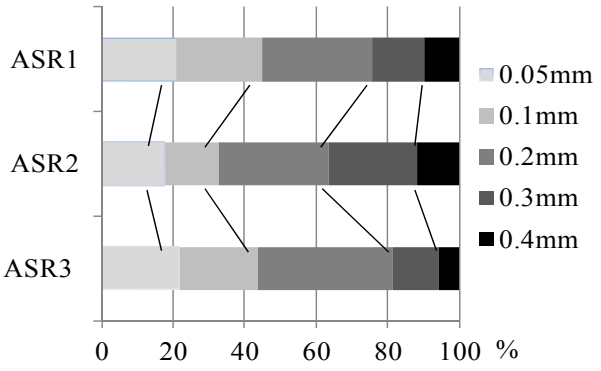

Figure 9: Comparison by the crack width

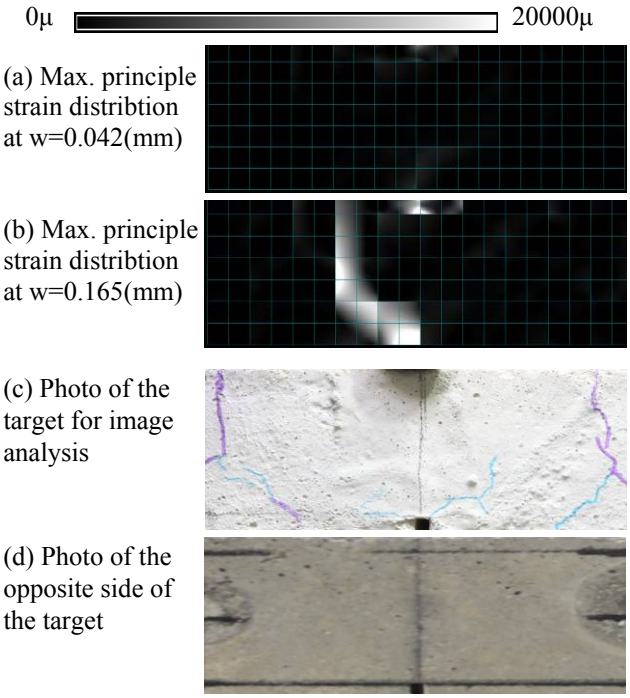

Figure 10: Distrribution of maximum principle strain obtained from the image analysis and photos of the target surface at the ligament of specimen ASR1

evaluated and classified into their widths, lengths and directions. Before performing the loading test, the crack width observed on the whole specimen was measured using a crack scale, and classified into the crack width of 0.05 mm, 0.1 mm, 0.2 mm, 0.3 mm and 0.4 mm, respectively. **Figure 8** shows total length and cross sectional area of ASR-induced cracks in each specimen. Here, the total cross sectional area of the cracks is assumed to be the summation of the products of a classified crack width and a total crack length within the range of the target crack width. **Figure 9** shows the proportion of classified crack width to the total in each specimen. The results indicate that although the total length of crack in the specimen ASR2 is shortest, the total cross sectional area of the cracks becomes larger in the all specimens. This is because that the ratio of cracks having the crack width of more than 0.2mm is largest in the specimens as shown in **Figure 9**. In addition, it seems reasonable to suppose that for the ASR induced crack when the total cross sectional area of the cracks is larger, the value of G_F tends to become smaller.

3.4 Maximum principal-strain distribution

Figure 10 shows the distribution of the maximum principal strain in the specimen ASR1 as a result of the image analysis. The result of the image analysis is shown with the fictitious crack width, w (mm). The picture of the ligament portion in this figure is of that before loading and domain as the image analysis target (100 mm in width, 50 mm in height). In the previous study [3], it has been confirmed that the crack to occur under external loading propagated along ASR-induced crack existing around the notch tip in the ligament of the notched beam. In addition, the ASR-induced crack that has existed horizontally at the notch tip opened with the increase in the external force. However, in this experiment, although the ASR-induced crack existed around the notch tip where the crack width was around 0.05 mm, the ASR-induced crack still closed under the flexural loading. From these results, in order to evaluate the

influence of the ASR-induced crack on the fracture properties of the concrete, an evaluation on the state of the ASR-induced crack at the ligament portion is needed. Moreover, it is necessary to consider the three-dimensional distribution of the ASR-induced cracks inside of the concrete.

4 CONCLUSIONS

In this study, the influence of the ASR-induced cracks on the tension-softening behavior of the concrete is experimentally evaluated. The three-point bending test for single notched concrete beams was carried out and the fracture energy and tension-softening curves of the ASR damaged concrete were obtained. To detect the crack propagation behavior, the image analysis by using a digital image correlation method was carried out during the loading. The conclusions obtained in the present study are as follows:

1) In the determination of the tension-softening curve calculated by the extended J-integration method, it is necessary to accurately evaluate the energy consumed in the fictitious-crack and the elastic energy release of the bulk portion except for the ligament.
2) The crack width observed on the whole specimen was measured and classified into the several crack widths respectively. It seems reasonable to suppose from the results of the fracture energy, G_F that for the ASR induced crack when the total cross sectional area of the cracks is larger, a value of G_F tends to become smaller.
3) The experiments show that the ASR induced cracks visible on the concrete surface do not always affect on the crack propagation occurred under the external loading. From these results, in order to evaluate the influence of the ASR-induced crack on the fracture properties of the concrete, an evaluation on the state of the ASR-induced crack at the ligament portion is needed. Moreover, it is necessary to consider the three-dimensional distribution of the ASR-induced cracks inside of the concrete.

Acknowledgements:

This research was partially supported from the Japan Society for the Promotion of Science (JSPS), Grant-in-Aid for Scientific Research (A) (JSPE KAKENHI Grant #22246061).

REFERENCES

[1] Kubo, Y., Ueda, T., Kuroda, T and Nomura, N., 2006. Influence of ASR expansion on mechanical properties of concrete. *J. of Japan Concrete Institute*, **28**(1), 1691-1696.

[2] Miki, T. and Nishino, Y., 2010. Experimental Study on Compressive Failure Features of Concrete Cracked Due to Alkali-Silica Reaction. *Proc. of the Concrete Structure Scenarios*, **10**, 187-192.

[3] Matsutani, K. and Miki, T., 2011. Fundamental Study on Tension Softening Behavior of Concrete Cracked Due to Alkali-Silica Reaction. *Proc. of the Concrete Structure Scenarios*, **11**, 479-484.

[4] Miki, T. and Hayashi, D., 2010. Measurement of the Strain Distribution of Concrete Subjected to Localized Compression by Using Image Correlation Method. *Memoirs of Const. Eng. Research Institute Foundation*, **52**, 53-60.

[5] Scharstein, D. and Szeliski, R., 2002. A Taxonomy and Evaluation of Dense Two-Frame Stereo Correspondence Algorithms. *Int. J. of Comp. Vision*, **47(**1-3), 7-42.

[6] Shimizu, M. and Okutomi, M., 2005. Sub-pixel Estimation Error Cancellation on Area-based Matching. *Int. J. of Comp. Vision*, **63**(3), 207-224.

[7] Kitsutaka, Y., Kamimura, K. and Nakamura, S., 1993. Poly-linear Approximation Analysis of Tension Softening Diagram for Concrete, *J. of Structural Construction Engineering*, **453**, 15-23.

[8] Niwa, J., Sumranwanich, T. and Matsuo, T., 1998. Experimental Study to Determine the Tension Softening Curve of Concrete. *J. of Materials, Concrete Structures and Pavements*, **606**(V-41), 75-88.

[9] Uchida Y., Rokugo, K. and Koyanagi, W., 1991. Determination of Tension Softening diagrams of Concrete by Means of Bending Tests. *J. of Materials, Concrete Structures and Pavements*, **426**(V-14), 203-212.